Laparoscopic ultrasound manipulator with a spring-based elastic mechanism

Arata, Jumpei
Department of Mechanical Engineering, Faculty of Engineering, Kyushu University

Fukami, Kazunari
Department of Engineering Physics, Electronics and Mechanics, Nagoya Institute of Technology

Oguri, Susumu
Department of Advanced Medical Initiatives, Faculty of Medical Sciences, Kyushu University

Onogi, Shinya
Center for Advanced Medical Innovation, Kyushu University

他

出版情報：International Journal of Computer Assisted Radiology and Surgery. 13, pp.1063-1072, 2018-02-28. Springer
バージョン：
権利関係：

J Arata, K Fukami, S Oguri, S Onogi, T Ikeda, R Nakadate, M Sakaguchi, T Akahoshi, K Harada, M Mitsuishi, M Hashizume: Laparoscopic Ultrasound Manipulator With a Spring-Based Elastic Mechanism, Int J CARS, Vol. 13(7), 1063-1072, 2018.

Laparoscopic Ultrasound Manipulator With a Spring-Based Elastic Mechanism

Jumpei Arata · Kazunari Fukami · Susumu Oguri · Shinya Onogi · Tetsuo Ikeda · Ryu Nakadate · Masamichi Sakaguchi · Tomohiko Akahoshi · Kanako Harada · Mamoru Mitsuishi · Makoto Hashizume

Received: date / Accepted: date

Abstract Purpose: Image guidance is a key technology that can improve the outcome of laparoscopic surgery. However, due to the large deformation caused by digestive organs, a computer-aided navigation system based on preoperative imaging data cannot indicate the correct target position of the lesion (e.g., liver tumors and vessels invisible from the organ surface). To overcome this issue, we developed a laparoscopic ultrasound manipulator with two motorized degrees of freedom at the tip, allowing for the performance of a dexterous ultrasound scan in a confined laparoscopic surgical area.
Method: The developed manipulator consists of a compact and elastic structure using springs, enabling a safe ultrasound scan and avoiding excess force on the inspected organs. The manipulator is a hand-held device equipped with four buttons at the handle, which the surgeon directly grasps to send a motion command to the tip structure. The tip of the manipulator was carefully designed by considering the kinematic model and the results of the finite element analysis. The developed prototype realizes two motorized degree of freedom

J. Arata
Department of Mechanical Engineering, Faculty of Engineering, Kyushu University
Motooka 744, Nishi-ku, Fukuoka 819-0395, Japan
Tel.: +81 92 802 3171 Fax: +81 92 802 0001 E-mail: jumpei@mech.kyushu-u.ac.jp

J. Arata, R. Nakadate, S. Onogi and M. Hashizume
Center for Advanced Medical Innovation, Kyushu University, Japan

S. Oguri, T. Akahoshi, T. Ikeda and M. Hashizume
Department of Advanced Medical Initiatives, Faculty of Medical Sciences, Kyushu University, Fukuoka, Japan

K. Fukami and M. Sakaguchi
Department of Engineering Physics, Electronics and Mechanics, Nagoya Institute of Technology, Nagoya, Japan

J. Arata, K. Harada and M. Mitsuishi
Department of Mechanical Engineering, Graduate School of Engineering, The University of Tokyo, Japan

motion at the tip within the size of 15.0 mm in diameter.
Results: To assess the prototype, accuracy and rigidity were measured by using a motion processing microscope. The accuracy test showed that the proposed device has a fairly accurate characteristic as a hand-held device. This was supposedly caused by the nature of compliant mechanism, which does not have mechanical play in motion. In addition, the intrinsic elastic structure (approximately 2.0 N/mm in most of the range of motion) allowed the ultrasound probe to adequately fit on the curved organ surface without extra effort of manipulation during the inspection. In the in vivo experiment, the yaw motion was found to be effective for investigating the vascular network because the manipulator allows the probe to be rotated while maintaining the same position.
Conclusion: The mechanical evaluation and in vivo tests results showed high feasibility of the prototype. We are currently working on further mechanical improvement for commercialization and development of a real-time navigation system that can perform three-dimensional reconstruction of ultrasonographic images by implementing a magnetic position sensor at the tip of the manipulator.

Keywords Laparoscopy · Laparoscopic Ultrasound · Robotic surgery · Handheld device

1 Purpose

Laparoscopic surgery requires surgeons to have high technical skills because of the limitations of instruments (small range of instrument motion, lack of haptic feedback, deteriorated eye-hand coordination, and poor depth perception). Image guidance is a key technology that can improve the outcome of laparoscopic surgery. However, because of the large deformation and displacement caused by the digestive organs, a computer-aided navigation system based on preoperative imaging data cannot indicate the correct target position of a lesion. One such example is when a liver tumor or vessels are invisible from the liver surface. Thus, image guidance can be a powerful tool for laparoscopic hepatectomy by ensuring visibility of the dissection area. However, the liver becomes largely deformed and displaced, and the preoperative images are no longer consistent with the intraoperative posture and position of the liver. Therefore, most laparoscopic surgeries are generally performed without a computer-aided navigation system and are thus largely reliant on the surgeon's skill [2]. However, a navigation system can potentially be an effective tool with which to improve the surgical outcome. To address this problem, we developed a laparoscopic ultrasound (LUS) manipulator that can perform dexterous motion with two motorized degrees of freedom (DOF), allowing for intraoperative and real-time image acquisition in laparoscopy.

The use of ultrasound (US) in laparoscopy is increasing, and guidelines for the use of LUS were provided by the Society of American Gastrointestinal

and Endoscopic Surgeons (SAGES) in March 2009 [3]. In these guidelines, different levels of recommendations are provided depending on the target organ (gastric cancer, esophagogastric cancer, adrenal surgery, biliary disease, gynecologic procedures, kidney disease, liver disease, and pancreatic disease). As an initial pilot study, we used the proposed device during liver surgery according to the following recommendation: "LUS is useful for staging of hepatocellular and metastatic colon and rectal cancers and can help guide treatment or avoid unnecessary open operations (Grade B) and detect metastasis from other cancers (Grade C)."

Despite the expected improvement in outcomes, LUS is not widely applied in liver surgery because of the limitations of commercially available instruments. Two types of probes are currently available for LUS: tethered and articulated probes. The tethered probe (e.g., UST-5418; Hitachi Medical, Tokyo, Japan) is a compact US probe that can be inserted to the abdominal cavity through a trocar and should be manipulated by conventional laparoscopic instruments, such as forceps. Therefore, the manipulation required for scanning a curved organ surface is technically demanding. The articulated probe is a laparoscopic tool equipped with one or more articulations and contains an US probe at the tip. The articulated probe (e.g., UST-9150; Hitachi Medical) has an advantage with respect to movement in multiple DOF within the abdominal cavity. However, this movement is largely limited by the number of articulations and location of the rotation center. Figure 1 shows the limitations of the articulated probe compared with an US scan on a patient's skin surface, which is generally performed in the clinical setting. In an US scan performed on the patient's skin surface, the inspector generally pivots the probe while maintaining contact with the skin, and the rotation center stays at the probe contact point to keep the probe position in the area of interest (Figure 1 (a)). The tip of the articulated probe moves mainly according to the movement of the articulations, making it difficult to keep the probe within the area of interest during inspection. This largely affects the usability of the probe because the inspection becomes difficult and cumbersome (Figure 1 (b)). To overcome these limitations, we developed a new LUS manipulator that can effectively manipulate the US probe in laparoscopic surgery for wider use.

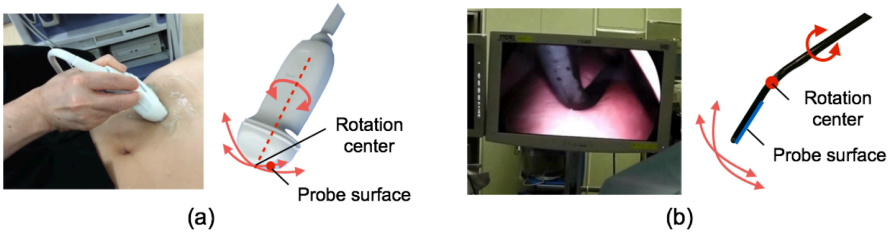

Fig. 1 (a) Ultrasound scan performed on the patient's skin surface allows for ideal motion, while (b) the articulated probe allows for only restricted movement due to the instrument limitation, making the inspection difficult and cumbersome (b).

2 Method

2.1 Technical requirements

One of the largest advantages of US as an image guidance modality in surgery is its real-time image acquisition. Therefore, the manipulator was designed as a handheld device that can be quickly introduced into the surgical area and retracted in the same manner. As described in the previous section, the largest limitations of the currently available LUS instruments are caused by the kinematic design of the articulations. To resolve this issue, we developed a new mechanism that ensures that the rotation center stays at the contact point of the US probe.

The remote center of rotation (RCM) has been widely discussed in the field of robotics. The RCM provides a remotely located rotation point, which is beneficial in certain applications such as the use of surgical robots. For example, the parallelograms implemented in the Da Vinci surgical robot provide a mechanical pivot point remotely located at the laparoscopic tool insertion point [8]. However, implementation of an RCM point in a compact, tube-shaped surgical instrument is challenging because of the size restriction. In addition, six DOF are required to freely position the US probe in three-dimensional space. Four DOF can be manually provided by the user's handle motion (two-DOF pivot, longitudinal, and rolling (twisting) motion); thus, two additional DOF of rotation with the RCM at the tip are required.

Few LUS products are available in the current market [9], [10]. The size of the US probe largely affects the image quality; thus, we choose an L43K (Hitachi Medical) in our prototype implementation. The diameter of the probe is 12.8 mm; thus, the manipulator should be less than 2.2 mm in thickness to be fitted into the standard 15-mm trocar. This represents the greatest technical challenge from the robotic aspect.

In LUS, the probe must be pushed against the inspected organ to obtain a clear US image. Therefore, a certain amount of elasticity in the manipulator's structure is desired to prevent excess force on the organ surface. We determined that the required stiffness of the manipulator was less than 10 N/mm, taking into consideration the stiffness of the liver [11].

A list of requirements for the LUS manipulator is shown below.

- Handheld implementation
- RCM at the contact point of the US probe
- Two DOF at the tip of the manipulator
- Compact and low-profile tip mechanism design (<2.2 mm thick at the thinnest part)
- An elastic structure is preferable to prevent damage (<10 N/mm in stiffness)

2.2 Prototype implementation

The prototype LUS manipulator is a hand-held device with a handle equipped with four buttons that the surgeon directly grasps to send a motion command to the tip mechanism (Figure 2). In the prototype implementation, a probe with a 12.8-mm diameter (L43K; Hitachi Aloka Medical, Tokyo, Japan) was used. The tip of the manipulator can be inserted through a conventional 15-mm trocar. The tip consists of biocompatible materials (stainless steel and nickel titanium) and can be detached by a snap-on mechanism (Figure 3). The handle was designed with consideration of the user's ergonomics [12]. Two motors (DCX12L + GPX12 + ENX10; Maxon Motor AG, Sachseln, Switzerland) are implemented in the handle part and driven by electric circuits implemented in the external control unit. The control unit is equipped with motor driver circuits, and a speed control dial and position initialization button are installed at the front. The LUS manipulator is 572 mm long, 56 mm wide, and 193 mm high, and the insertion part is 370 mm long and 15 mm in diameter. The weight is approximately 800 g.

The tip of the manipulator is associated with notable features and technical challenges. A detailed description of this is provided in the following section.

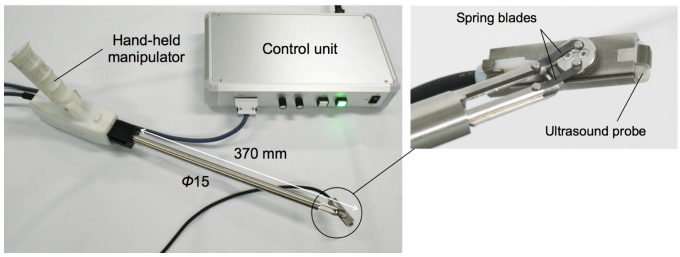

Fig. 2 The prototype consists of a handheld laparoscopic ultrasound manipulator and an ultrasound control box. A commercialized laparoscopic ultrasound probe (L43K; Hitachi Medical) can be attached to the tip of the manipulator.

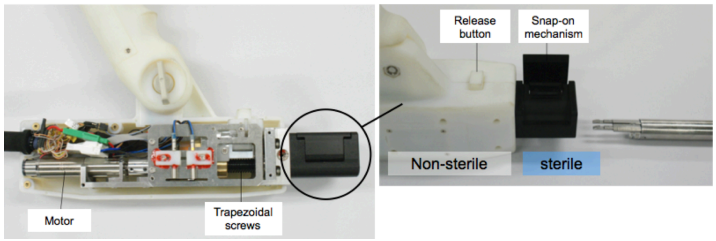

Fig. 3 Two motors are implemented in the handle part and driven by the electric circuits implemented in the control box. The tip part consists of biocompatible materials (stainless steel and nickel titanium) and can be detached by a snap-on mechanism.

2.3 Mechanism design

A newly developed spring-based elastic mechanism at the tip performs rotational motion in two degrees of freedom (pitch and yaw as shown in Figure 4). Two rigid links that are independently actuated along the long axis are connected to the flat springs by passive rotational joints. The other ends of the springs are attached by passive joints to a circular plate that rotates along with a yaw axis guided by sliding bearings. The pitch axis is guided by a mechanical hinge implemented at the tip. The movement of the two flat springs in the same direction is converted to pitch motion, and differential movement is converted to yaw motion. Figure 5 shows the motion performed by the prototype.

A notable feature of the proposed mechanism is the elastic elements embedded in the mechanical frame. These elements largely deform in motion to transmit and transform the input motion to output motion. This substantially contributes to simplification of such mechanical instruments [5], [6]. A previous study [4] showed that rotational motion with the probe contact plane centered at the probe contact point (yaw axis) is effective in LUS, although the motion cannot be performed using the conventional LUS articulated probe. In

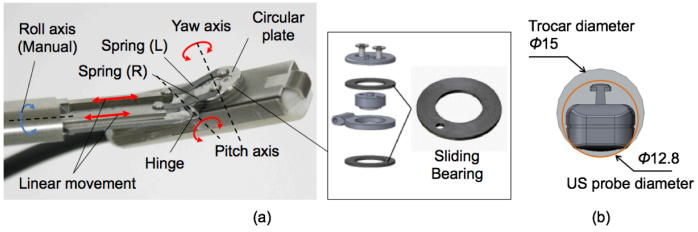

Fig. 4 (a) The mechanism performs rotational yaw and pitch motion in two degrees of freedom through transfer of the two linear movements by the elastic mechanism at the tip. (b) The thinnest part of the mechanism is 2.2 mm, allowing it to be fitted to a conventional 15-mm trocar.

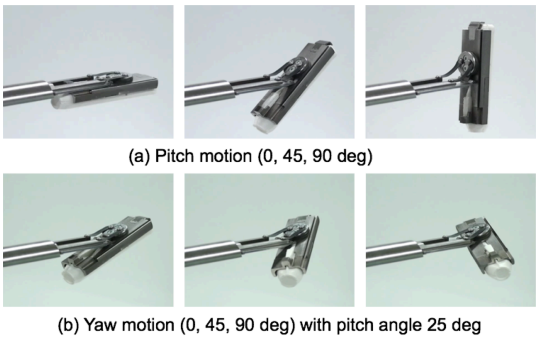

Fig. 5 (a) The pitch motion is performed by moving the two spring blades in the same direction. (b) The yaw motion can be performed by moving the two spring blades in different directions.

addition, based on the ideal approach angle reported for US inspection [7], we determined that the required working range is ±90 degrees in the yaw axis and 0 to 90 degrees in the pitch axis (0 degrees in both pitch and yaw when the tip is straightened). Notably, the yaw motion is only allowed at a pitch angle of equal or larger than 20 degrees to avoid a physical collision between the fixture notch on the US probe and the manipulator.

The spring was designed to fulfill the design criteria for maximization of the working area. Figure 6 shows the three conditions taken into account for the design, considering the yaw motion. First, (a) the two spring blades must not collide with each other while in motion. Second, (b) the singularity point regarding the kinematic model must be avoided. Finally, (c) because the pitch rotation axis is located below the two spring blades, elastic parts must remain on the axis, allowing rotation by deformation of both spring blades. We also performed a series of finite element analyses (FEAs) with the model meshed by a hexahedron using FEMAP Ver. 10.0.2 (Siemens PLM Software, Plano, TX, USA). As a representative example, FEA was performed by DAFUL Ver. 5.0 (Virtual Motion, Seoul, Korea.). The optimized spring is shown in Figure 8. The spring should be designed to not exceed the yield strain of the material (7 %) to prevent damage that may cause breakage. We simulated the position in which the springs were strained at maximum with different spring thicknesses. The results revealed that the maximum strain appeared to be 6.46 % when the spring thickness was configured at 0.2 mm (9.16 % and 14.7% when the spring thickness was 0.3 mm and 0.4 mm, respectively). Therefore, we determined that a spring thickness of 0.2 mm that was ideal for the prototype design because the maximum strain was smaller than the yield strain.

Two flat springs (0.2 mm in thickness) were fabricated from nickel titanium alloy to allow a high degree of deformation. Notably, the deformation of the two flat springs is guided by two mechanical hinges attached at the tip on each DOF; thus, each spring adequately deforms as precalculated in the FEA. The working range is 20 to 90 degrees in the pitch axis and +90 to −90 degrees in the yaw axis, also as precalculated in the FEA.

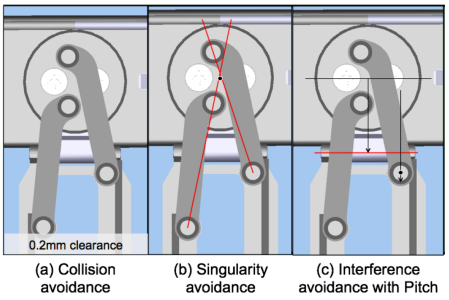

Fig. 6 These images show the three conditions taking into account the spring design in terms of yaw motion. (a) The two spring blades must not collide with each other when in motion. (b) The singularity point regarding the kinematic model must be avoided. (c) Elastic parts must remain on the pitch rotation axis.

2.4 Kinematic modeling

To adequately control the manipulator's posture at the tip, an inverse kinematic model is required to compute the positions of the linear motors according to the desired angles in the pitch and yaw axes.

In pitch motion, the spring blades are largely deformed, and this deformation affects the kinematic model. When the two spring blades are moving in the same direction, pitch motion is generated at the tip. We thus performed an FEA analysis and obtained the inverse kinematic model by approximation using the fifth-degree equation because the coefficient of correlation between the FEA and the approximated model - R^2 was converged to 1.000 by the fifth-degree equation.

$$L_p = -4\theta^5 \times 10^{-10} + 7\theta^4 \times 10^{-8} - 6\theta^3 \times 10^{-6} + 3\theta^2 \times 10^{-4} + 3.36\theta \times 10^{-2} \tag{1}$$

where L_p is the displacement of linear motor from the initial position (pitch angle θ is 0 degrees when L_p is 0 mm).

The yaw angle is obtained by the geometric conditions of the two spring blades. When the two spring blades move in different directions, the mechanism performs a yaw motion. First, from the angles β and γ as shown in Figure 9, the following equations are derived:

$$\cos\beta = \frac{L_{yl} + \sqrt{l^2 + h^2 - (s - r\cos\delta)^2} + r\sin(\delta - \phi) - r\sin\delta - r\sin\delta}{\sqrt{l^2 + h^2}} \tag{2}$$

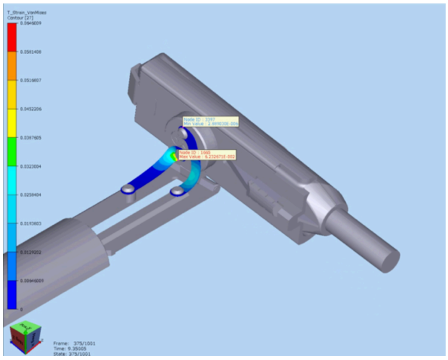

Fig. 7 This figure shows a representative example of the finite element analysis results. The motion of the pitch and yaw axes can be performed by simulating the spring deformations.

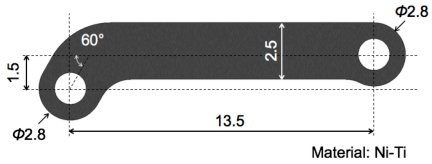

Fig. 8 The dimensions of the spring were determined by a series of finite element analyses.

$$\sin\beta = \frac{s - r\cos(\delta - \phi)}{\sqrt{l^2 + h^2}} \tag{3}$$

$$\cos\gamma = \frac{-L_{yl} + \sqrt{l^2 + h^2 - (s - r\cos\delta)^2} + r\sin(\delta + \phi) - r\sin\delta - r\sin\delta}{\sqrt{l^2 + h^2}} \tag{4}$$

$$\sin\gamma = \frac{s - r\cos(\delta + \phi)}{\sqrt{l^2 + h^2}} \tag{5}$$

where L_{yr} and L_{yl} are the displacements of the right and left linear motors from the initial position (yaw angle ϕ is 0 degrees when L_{yr} and L_{yl} are 0 mm), respectively. Other parameters are shown in Figure 9. By sum of squares of equations (2), (3) and (4), (5), we obtain:

$$l^2 + h^2 = \{L_{yl} + \sqrt{l^2 + h^2 - (s - r\cos\delta)^2} + r\sin(\delta - \varphi) - r\sin\delta\}^2 + \{s - r\cos(\delta - \varphi)\}^2 \tag{6}$$

$$l^2 + h^2 = \{-L_{yr} + \sqrt{l^2 + h^2 - (s - r\cos\delta)^2} + r\sin(\delta + \varphi) - r\sin\delta\}^2 + \{s - r\cos(\delta + \varphi)\}^2 \tag{7}$$

From Equations (6) and (7), the displacement of springs L_{yl} and L_{yr} for performing the yaw axis motion with the angle ϕ is obtained as follows:

$$L_{yl} = -\sqrt{l^2 + h^2 - (s - r\cos\delta)^2)} - r\{\sin(\delta - \phi) - \sin\delta\} + \sqrt{l^2 + h^2 - \{s - r\cos(\delta - \phi)\}^2} \tag{8}$$

$$L_{yr} = \sqrt{l^2 + h^2 - (s - r\cos\delta)^2)} + r\{\sin(\delta - \phi) - \sin\delta\} - \sqrt{l^2 + h^2 - \{s - r\cos(\delta - \phi)\}^2} \tag{9}$$

Note that L_{yl} and L_{yr} are symmetrical because the differential motion of L_{yl} and L_{yr} produces the yaw motion.

Finally, the target positions of L_l and L_r for performing the pitch and yaw motion with the angles of θ and ϕ are derived as follows:

$$L_l = L_p + L_{yl} \tag{10}$$

$$L_r = L_p + L_{yr} \tag{11}$$

Note that the kinematic model is derived from the pitch and yaw axes independently. Because a high pitch angle increases the deformation of both springs, the yaw motion is influenced by the pitch motion. This is examined and discussed in the following section.

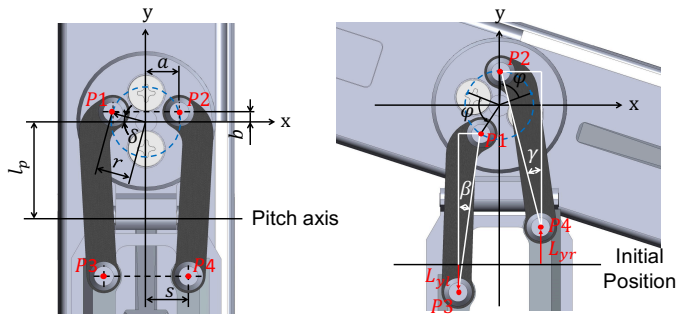

Fig. 9 This figure shows the parameter definitions used in the kinematic modeling.

2.5 Evaluations

We conducted a series of mechanical experiments to evaluate the accuracy and rigidity of the prototype. In addition, an in vivo experiment was performed on a pig to evaluate the overall utility.

2.5.1 Position accuracy test

Because the device is hand-held, its position accuracy largely affects its utility, especially in terms of repeat accuracy (e.g., the device is expected to accurately return to the original position when the surgeon gives the motion command). The test was performed in the both DOF (pitch and yaw motion).

Figure 10 shows the experimental setup for the mechanical evaluation. The prototype was firmly fixed onto the experimental rig while image markers were attached at the tip. The motion was performed while the tip was monitored by a motion processing microscope (VW-6000; Keyence Corporation, Osaka, Japan), and the recorded image was further processed as a trajectory. All motions were measured three times at a sampling rate of 250 frames per second. The accuracy of the measurement system employed in the experiment was 50 μm. The pitch and yaw motion were independently performed for each measurement. The pitch motion was performed from 0 (straightened) to 90 degrees. The yaw motion was performed in the range of $\pm$90 degrees, while the pitch angle varied (20, 45, and 90 degrees). Note that yaw motion was only allowed when the pitch angle was larger than 20 degrees to avoid mechanical collision between the manipulator and US probe.

2.5.2 Rigidity test

The proposed device manipulates the LUS probe to scan the organ surface. Thus, some degree of softness is needed to avoid damaging the organs. Few studies have been performed to assess the most appropriate force to be applied against the organs in LUS; however, we determined that the most desirable device rigidity for appropriate performance of LUS ranges from 1 to 10 N/mm, taking into account previously published work [11], [13].

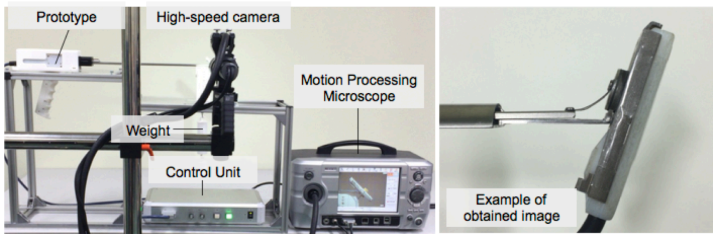

Fig. 10 Experimental setup for accuracy and rigidity tests.

The rigidity of the proposed device varies according to the motion caused by the spring deformations. We therefore measured the rigidity with the prototype in different postures (pitch angle varied from 20 to 90 degrees, while yaw varied at 0, ±30, ±60 and ±90 degrees). The rigidity was computed from the displacement observed while a 1.5-N load was applied at the tip. The measurements were performed using the same setup used in the accuracy test, and the load was applied by a force gauge. The measurements were performed three times in each position.

2.5.3 In vivo experiment

As a preliminary evaluation, we conducted an in vivo experiment on a pig. The prototype was inserted to the abdominal cavity, and a liver scan was performed while observing the surgical area with a laparoscope. The experiment was performed by experienced laparoscopic surgeons, and the ethical code for animal experimentation established by Kyushu University was strictly observed.

3 Results

3.1 Position accuracy test

The measured pitch and yaw motion trajectories are shown in Figure 11, and computed error regarding the rotational center from the trajectory is shown in Table 1. The pitch motion showed high accuracy with a mean error of 0.289 degrees, while the error in yaw motion increased as the pitch angle increased. This tendency was clearer for the larger angles of the yaw axis. These findings suggest that large deformation of the springs causes discordance between the kinematic model and actual deformation. However, the accuracy is generally good in compliant mechanisms because it does not contain conventional mechanical elements (e.g., pins and bearings) that cause mechanical play. The experimental result shown in Figure 11(b) supports this fact. This error can be further reduced by including this result in the kinematic model; however, as a hand-held device, the error seems to be sufficiently small. Repeat accuracy is expected to be a key factor for the utility of LUS because the user directly handles the device during the procedure. This issue is further evaluated and described in the in vivo experiment.

Table 1 Results of accuracy test

Motion	Angular mean error [deg]	Range of Motion [deg]
Pitch	0.289	from 0.453 to 90.0
Pitch20deg/Yaw±90deg	1.09	from -88.4 to - 89.6
Pitch45deg/Yaw±90deg	1.44	from -88.8 to - 88.2
Pitch90deg/Yaw±90deg	2.05	from -83.9 to 89.5

3.2 Rigidity test

The experimental results regarding the pitch and yaw axes are shown in Figure 12. The rigidity increased as the pitch angle increased, as shown in Figure 12(a). This was in accordance with the nature of a compliant mechanism; i.e., a large spring deformation increases the rigidity. The variation in the rigidity according to the yaw motion was mostly uniform at approximately 2.0 N/mm, except when the yaw angle was −90 degrees, in which case the rigidity was approximately four times stiffer. This was supposedly caused by a mechanical collision in the mechanical chain that unexpectedly occurred due to an assembly error. Overall, the rigidity was within the desirable range to avoid unexpected damage to the organs while allowing for accurate probing.

3.3 In vivo experiment

The pictures taken by the laparoscope during the procedure are shown in Figure 13. The result showed that the prototype could successfully perform

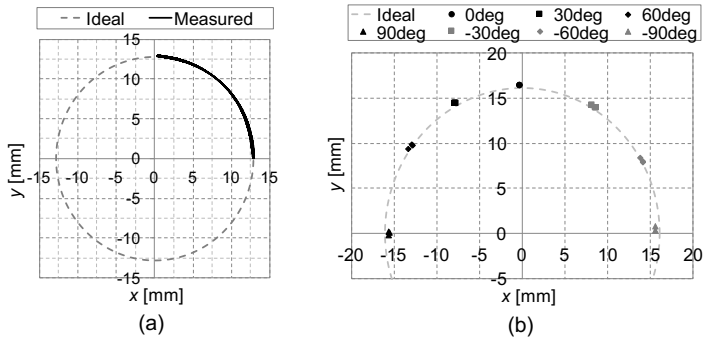

Fig. 11 Measured trajectory in the accuracy test. (a) Pitch motion. (b) Yaw motion.

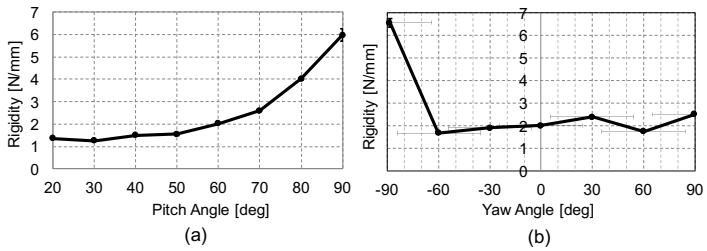

Fig. 12 (a) Result of rigidity test while pitch angle varied and yaw angle was fixed at 0 degrees. (b) Result of rigidity test while yaw motion varied and pitch angle was fixed at 20 degrees.

the US scan with both pitch and yaw motions. The intrinsic elastic structure of the prototype was found to be useful because it adequately fit the curved surface without taking extra care or risking an excess load on the phantom model. The rigidity of the manipulator was 1.69 N/mm at the initial position (pitch, 20 degrees; yaw, 0 degrees) when the load was applied against the US probe from the bottom.

A vessel localization task was also successfully performed in an in vivo test on a pig. Examples of US images taken in the in vivo experiment are shown in Figure 14. The obtained US image quality was fairly good for the inspection because the prototype could provide appropriate amount of pressure to be fitted on to the curved organ surface without taking extra care. The yaw motion was found to be highly effective for investigating the vascular network because the manipulator allowed the US probe to turn while maintaining the same position; the vessel could thus be seen from both the longitudinal and traverse section.

This motion cannot be performed by a conventional LUS probe. Thus, the feasibility of the prototype was shown.

4 Discussion and Conclusion

In this study, we evaluated the use of a laparoscopic US scan manipulator consisting of a newly developed spring-based elastic mechanism. The movement of

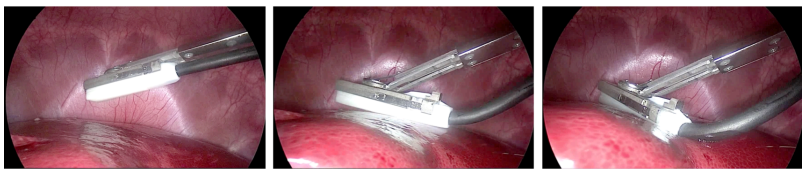

Fig. 13 The in vivo test demonstrated the feasibility of the prototype. (a) Approaching the target area. (b) Pitch motion performed to fit the prototype to the organ surface. (c) Yaw motion performed to search for hidden vessel networks in the liver.

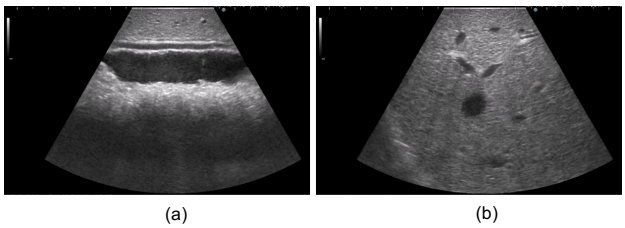

Fig. 14 Examples of US images taken in the in vivo experiment. (a) shows a longitudinal section of a vessel, and (b) shows a traverse section of a vessel.

the two flat springs allows the prototype to perform motion in two motorized DOF at the tip (pitch, yaw, and manual rotation along the long axis). The diameter of the prototype is 15.0 mm, and the LUS probe in the prototype is 12.8 mm in diameter. A notable feature of the proposed device is the new elastic mechanism. This mechanism allowed the low-profile design of the manipulator to be fitted into a 15-mm-diameter trocar together with the LUS probe. The accuracy test showed a fairly accurate characteristic as a hand-held device because the proposed mechanism does not have mechanical play. In addition, the intrinsic elastic structure allowed the US probe to adequately fit on the curved organ surface without extra effort of manipulation during the inspection. This avoids unexpected organ damage. In the in vivo experiment, the yaw motion was found to be effective for investigating the vascular network because the manipulator allows the probe to be rotated while maintaining the same position. This advantage would be useful in combination with a computer-aided navigation system. We are currently working on the development of a real-time navigation system that can perform three-dimensional reconstruction of ultrasonographic images by implementing a magnetic position sensor (Aurora; Northern Digital Inc., Waterloo, Ontario, Canada) at the tip of the manipulator [14], [15].

Acknowledgement

This research was supported by Japan Agency for Medical Research and Development (AMED), Research on Development of New Medical Devices (15hk0102005h0002).

Conflict of interest

Jumpei Arata, Kazunari Fukami, Susumu Oguri, Tetsuo Ikeda, Ryu Nakadate, Shinya Onogi, Masamichi Sakaguchi, Kanako Harada, Mamoru Mitsuishi, and Makoto Hashizume declare that they have no conflict of interest.

Human participants and/or animals

This article does not contain any studies with human participants performed by any of the authors. All procedures performed in studies involving animals were in accordance with the ethical standards of the institution or practice at which the studies were conducted.

References

1. Konishi K, Nakamoto M, Kakeji Y, Tanoue K, Kawanaka H, Yamaguchi S, Ieiri S, Sato Y, Maehara Y, Tamura S, Hashizume M (2007) A real-time navigation system for laparoscopic surgery based on three-dimensional ultrasound using magneto-optic hybrid tracking configuration, Int J CARS, 2:1-10.

2. Nicolau S, Soler L, Mutter D, Marescaux J (2011), Augmented reality in laparoscopic surgical oncology, Surgical Oncology, 20(3):189-201.
3. http://www.sages.org/publications/guidelines/guidelines-for-the-use-of-laparoscopic-ultrasound/ (2016)
4. Oguri S, Arata J, Ikeda T, Nakadate R, Onogi S, Akahoshi T, Harada K, Mitsuishi M, Hashizume M (2015) Multi-Degrees of Freedom Laparoscopic Ultrasound Probe with Remote Center of Motion, Int J CARS, 10(Suppl 1):S242-244.
5. Arata J., Kogiso S., Sakaguchi M., Nakadate R., Oguri S., Uemura M., Cho, B., Akahoshi T., Ikeda T., Hashizume M. (2015) Articulated minimally invasive surgical tool for laparoscopy based on compliant mechanism, Int J CARS, 10:1837-1843.
6. Arata J., Saito Y., Fujimoto H., (2010) Outer Shell Type 2 DOF Bending Manipulator using Spring-link Mechanism for Medical Applications, Proc. of Int. Conf. Robotics and Automation, 1041-1046.
7. Denadai R., Toledo A. P., Bernades D. M., Diniz F. D., Eid F. B., Lanfranchi L. M., Amaro L. C., Germani N. M., Parise V. G., Pacheco Filho C. N., Saad-Hossne R. (2014) Simulation-based ultrasound-guided central venous cannulation training program, Acta Cirurgica Brasileira, 29(2):132-144.
8. https://www.intuitivesurgical.com/products/da-vinci-xi/ (2017)
9. http://www.hitachi-aloka.com/applications/surgery/laparoscopic-surgery (2017)
10. https://bkultrasound.com/applications/surgery/laparoscopic-ultrasound-for-surgery/ (2017)
11. Sandrin L., Fourquet B., Hasquenoph J. M., Yon S., Fournier C., Mal F. Christidis C., Ziol M., Poulet B., Kazemi F., Beaugrand M., Palau R. (2013) Transient elastography: a new noninvasive method for assessment of hepatic fibrosis, Ultrasound in Med. & Biol., 29(12):1705-1713.
12. Sato H., Harada K., Arata J., Oguri S., Onogi S., Ikeda T., Hashizume M., Mitsuishi M. (2016) Design and prototyping of handheld 3-DOF laparoscopic ultrasound manipulator, Procedia CIRP, 49:121-124.
13. Takachi Y., Masuda K., Yasunaga T., Aoki Y. (2011) Development of Support System for Handling Ultrasound Probe to Alleviate Fatigue of Physician by introducing a coordinated motion with Robot, J Robotic Society of Japan, 29(7):634-642. (in Japanese)
14. Onogi S., Ikeda T., Arata J., Nakadate R., Oguri S., Akahoshi T., Harada K., Mitsuishi M., Hashizume M. (2016) Intra-operative three dimensional ultrasound reconstruction and visualization for endoscopic liver surgery, Int J CARS, 11(Suppl 1):S256-257.
15. Onogi S., Nakadate R., Arata J., Akahoshi T., Ikeda T., Hashizume M. (2017) Technical trial of GPGPU volume reconstruction by using a tablet PC for practical clinical navigation system, Int J CARS, 12(1):S96-97.